



# CHORUS

This is the accepted manuscript made available via CHORUS. The article has been published as:

## Field-Induced Electron Spin Resonance of Site-Selective Carrier Accumulation in Field-Effect Transistors Composed of Organic Semiconductor Solid Solutions

Hiroyuki Matsui, Eiji Takahashi, Seiji Tsuzuki, Kazuo Takimiya, and Tatsuo Hasegawa

Phys. Rev. Applied **16**, 034019 — Published 10 September 2021

DOI: [10.1103/PhysRevApplied.16.034019](https://doi.org/10.1103/PhysRevApplied.16.034019)

# Field-Induced Electron Spin Resonance of Site-Selective Carrier Accumulation in Field-Effect Transistors Composed of Organic Semiconductor Solid Solutions

Hiroyuki Matsui\*

*Research Center for Organic Electronics (ROEL), Yamagata University, Jonan 4-3-16, Yonezawa, Yamagata, 922-8510, Japan*

*E-mail: h-matsui@yz.yamagata-u.ac.jp*

Eiji Takahashi

*Osaka Laboratory, Sumika Chemical Analysis Service, Ltd., 1-135, Kasugade-Naka 3-chome, Konohana-ku, Osaka, 554-0022, Japan*

Seiji Tsuzuki

*Department of Applied Physics, The University of Tokyo, Hongo 7-3-1, Bunkyo-ku, Tokyo, 113-8656, Japan*

Kazuo Takimiya

*Department of Chemistry, Tohoku University, 6-3, Aramaki Aza-Aoba, Aoba-ku, Sendai, 980-8578, Japan*

Tatsuo Hasegawa\*

*Department of Applied Physics, The University of Tokyo, Hongo 7-3-1, Bunkyo-ku, Tokyo, 113-8656, Japan*

*E-mail: t-hasegawa@ap.t.u-tokyo.ac.jp*

The formation and characterization of solid solutions with guest (or impurity) molecules are difficult to realize in crystalline organic semiconductors. Here, we demonstrate that an operando field-induced electron spin resonance (FI-ESR) experiment allows the site-selective analysis of accumulated charge carriers in polycrystalline organic field-effect transistors (FETs), which comprise molecular solid solutions as channel semiconductor layers. We utilize vacuum-deposited dinaphtho[2,3-*b*:2',3'-*f*]thieno[3,2-*b*]thiophene (DNNT) thin films with various amounts of dibenzo-tetrathiafulvalene (DBTTF) as guest molecules. Our measurements reveal that the field-induced carriers are first trapped at guest DBTTF sites at low gate voltages and then begin to accumulate at host DNNT sites at higher

gate voltages. Furthermore, we perform dispersion-corrected density functional theory calculations to investigate the stability of the solid-solution crystals. It is shown that the DBTTF molecules can be stably incorporated by aligning molecular long axes within the crystal lattices of DNNT, the results of which agree well with the angle-dependent FI-ESR measurements. We demonstrate that the mobility, threshold voltage, and subthreshold swing are controlled by the concentration of guest molecules in solid-solution organic FETs.

## I. INTRODUCTION

The physics of organic semiconductors that can be utilized in light-emitting devices, photovoltaics, and field-effect transistors (FETs) has been investigated intensively in recent decades [1-4]. Amorphous organic semiconductors are preferable for light-emitting devices and photovoltaics, whereas crystalline organic semiconductors are preferable for FETs owing to their relatively high mobility. Recent progress in crystalline organic semiconductors indicate that field-effect mobilities can exceed  $10 \text{ cm}^2/\text{Vs}$ , as reported in several reliable experimental studies [5]. It is demonstrated that highly ordered layered molecular packing is essential for obtaining the enough high performance. In this context, methods for impurity doping, which is known to be a primary basis in mature inorganic silicon technology, are hardly compatible with the high mobility organic semiconductors. Actually, it was discussed that doping has a strong influence on the packing structure of most crystalline molecular materials, which eventually leads to the reduction in carrier mobility [6]. The feature is related to the fact that organic semiconductor crystals are composed of molecules with specific shape, size, orientation and conformation, which makes it unstraightforward to incorporate the other kinds of guest species within the crystal lattices that are weakly bound together and are grown at around room temperature. Hence, crystalline organic semiconductors are typically utilized as intrinsic semiconductors in high-mobility organic FETs. Thus the important challenge in high mobility organic FETs is to realize doped organic semiconductors with keeping both the crystalline order and high mobility [6].

Solid-solution crystals composed of two different types of molecules can be manufactured using a specific combination of molecules. The molecular solid solution is defined as a mixed crystal, in which host molecules are randomly replaced by guest molecules in the crystal lattices, like doped silicon. Solid solution is clearly different from mixed amorphous or phase-separated films, in that it keeps the periodicity of the host crystal lattices with maintaining the mesoscopic homogeneity. Hence, it should facilitate the continuous tuning of semiconducting properties. Hinderhofer and Schreiber reported that when two types of molecules (A and B) are mixed to form crystalline thin films via vacuum deposition, the films obtained can be classified into the following three categories: ordered complex, phase separation, and solid solution [7]. A solid solution can be achieved when the magnitude of the intermolecular interaction between different molecules (A–B) is comparable to those in pure

systems (A–A or B–B). Several combinations of semiconducting molecular species have been reported to form solid solutions: H<sub>16</sub>CuPC:F<sub>16</sub>CuPc [8], pentacene:picene [9], pentacene:diindenoperylene [10], pentacene:*p*-terphenyl [11], 6,13-bis(triisopropyl-silylethynyl)pentacene: 6,13-bis(triisopropyl-silylethynyl)tetraazapentacene [12], and C6-BTBT:C10-BTBT [13]. Furthermore, these solid solutions were investigated via X-ray diffraction [8-10] or in photo-induced electron spin resonance (ESR) studies [11]. The use of solid solutions for organic FETs may allow the continuous tuning of device characteristics by varying the amount of guest molecules involved in the channel of organic semiconductors. In addition, the manner how the guest or impurity molecules affect the device characteristics must be understood to optimize the FET characteristics. However, the effect of using a molecular solid solution on gate-induced carrier accumulation has not been investigated hitherto for organic FETs. This is mainly because it is quite difficult to characterize the amount of guest molecules in the channel organic semiconductors, and thus to correlate it with the FET characteristics.

In this study, we demonstrate that an operando field-induced electron spin resonance (FI-ESR) experiment can be utilized to investigate the effects of guest molecule doping on gate-induced carrier accumulation in solid-solution organic FETs. The FI-ESR technique has been utilized as a unique and useful microscopic tool to probe carrier dynamics as well as trap-induced carrier localization by detecting the radical 1/2-spin of gate-induced carriers, as has been demonstrated for several small-molecule and polymer-based organic FETs [14-24]. In this study, we utilized polycrystalline solid-solution thin films based on dinaphtho[2,3-*b*:2',3'-*f*]thieno[3,2-*b*]thiophene (DNTT), which is a well-known air-stable and high-performance organic semiconductor, as a host crystalline material [25, 26]. The results of FI-ESR measurements indicate that vacuum-deposited DNTT films can host dibenzotetrathiafulvalene (DBTTF) [27] as guest molecules in their crystal lattices. Gate-voltage-dependent and angle-dependent FI-ESR spectroscopy allows the site-selective analysis of accumulated charge carriers; hence, the energy level alignment and molecular orientation of the guest DBTTF molecules in the host DNTT crystals can be determined. Herein, we discuss why DBTTF molecules can be stably incorporated within the crystal lattices of DNTT based on dispersion-corrected density functional theory (DFT) calculations to ensure the stability of solid-solution crystals. Finally, we present the concentration dependence of FET characteristics in terms of the formation of trap sites by guest molecules, where the controllability of the FET characteristics is discussed.

## II. METHODOLOGY

### A. Fabrication of solid-solution FET

A schematic illustration of solid-solution organic FETs is shown in Fig. 1a. A polyethylene naphthalate sheet (100 μm thick, TEONEX Q65F, Dupont) cut into a width of 3 mm and a length of 400 mm was used as a substrate to fit the ESR tube. A gold gate electrode (30 nm thick), a parylene C dielectric layer (1 μm thick), a solid-solution channel semiconductor layer, and gold source and drain

electrodes (30 nm thick) were successively deposited on the substrate. All device fabrication and measurements were performed in an argon atmosphere.

The channel layer was fabricated via the co-evaporation of DNNT and DBTTF from independently temperature-controlled crucibles. The deposition rate of the host DNNT was set at 0.04 nm/s, whereas that of the guest DBTTF was controlled to obtain various concentrations between 0.01% and 0.75%. The concentration of DBTTF was determined via FI-ESR measurements. It was unknown that the combination of DNNT and DBTTF yielded solid solutions, although the guest DBTTF molecule exhibits a shape and size similar to those of the host DNNT molecule, as presented in Fig. 1b. The present FI-ESR study confirmed the formation of solid solutions with dilute concentrations of DBTTF as low as 0.01%, as will be discussed later.

## B. Operando FI-ESR technique

FI-ESR measurements were performed using a standard X-band ESR apparatus (JES-FA200, JEOL) and a semiconductor parameter analyzer (E5270A, Agilent). The devices prepared were inserted and sealed in quartz tubes for both FI-ESR and FET characteristic measurements. The angle-dependent ESR spectra were measured by rotating the ESR tube on its axis, where the relative angle between the static magnetic field and the film plane was adjusted using a protractor. A continuous-flow cryostat was used for the low-temperature measurements. We used 2,2-diphenyl-1-picrylhydrazyl (DPPH) as a reference for the ESR signal and a manganese marker ( $\text{MgO}/\text{Mn}^{2+}$ ) as a subsidiary standard.

In the FI-ESR measurements, the anisotropic molecular  $g$  tensor was the key parameter, which is useful for discriminating the species and orientations of molecules at which carriers are accumulated; the  $g$  tensor is defined as  $g = h\nu/\mu_B B$ , where  $h$  is the Planck constant,  $\nu$  the microwave frequency,  $\mu_B$  the Bohr magneton, and  $B$  the static magnetic field. A comparison of the obtained  $g$  values allowed us to identify the molecular species. In addition, the analysis of the angle dependence of the  $g$  factor enabled the determination of the molecular orientation on the substrate. The gate-induced carrier density at the respective molecular sites can be determined by integrating the ESR signal at each gate voltage.

## C. DFT calculation

We used Gaussian 16 for the DFT calculations [28] of both the molecular  $g$  tensor and intermolecular interaction energies. The former calculation was performed at the unrestricted B3LYP/6-31G(d,p) level using the molecular structures at the cationic state optimized at the same level. The intermolecular interaction energies were calculated at the B3LYP/6-311G(d,p)//B3LYP/6-31G(d) level with Grimme's D3 dispersion correction [29]. The basis set superposition error [30] was corrected using the counterpoise method [31]. The crystal structure of the solid solution was prepared

by replacing the central DNTT molecule with a guest DBTTF molecule. The geometry and position of the central DBTTF molecule were optimized at the same level with six fixed DNTT molecules.

### III. RESULTS AND DISCUSSION

#### A. Operando ESR observation for site-selective carrier accumulation

Figure 2a shows the field-induced ESR spectra of a DNTT (99.8%): DBTTF (0.2%) solid-solution FET at room temperature. A static magnetic field was applied perpendicular to the substrate. Two types of signals were observed at lower and higher magnetic fields, which are referred to as signals I and II, respectively. Signal I began to increase at gate voltage  $V_G = -40$  V and saturated at approximately  $-100$  V (Fig. 2b). By contrast, signal II began to increase at  $V_G = -80$  V and did not saturate down to  $-200$  V. Because the difference in the resonance magnetic fields was derived from the difference in the  $g$  factors, the molecular species or orientations between the two signals were different.

Figures 3a–c show the angular dependence of the  $g$  factors for signals I and II. The appropriate gate voltages and preset temperatures were selected to measure the respective signals (100 K for signal I and room temperature for signal II). The high temperature imposed two different effects on the spectral line shape, as reported previously<sup>19</sup>. The first effect was the decrease in the spin-lattice relaxation time, which broadened the spectral line width. The second was the motional narrowing effect, which averaged out the different  $g$  values of randomly oriented crystalline domains. Because of these effects, the ESR spectra must be measured at low temperatures to resolve the  $g$  values of the respective crystalline domains. Both signal I and II exhibited typical tendencies of the largest single  $g$  factor at  $\theta = 90^\circ$  and the powder pattern due to the random orientation of crystals at  $\theta = 0^\circ$ . By fitting the spectra at  $\theta = 0^\circ$  with a theoretical powder pattern, we extracted two principal  $g$  factors, as shown in Table I. The  $g$  shift of signal I from the free electron value ( $g_e = 2.0023$ ) was almost twice that of signal II. Moreover, the angular averages  $g_{ave} = (g_x + g_y + g_z)/3$  of the two signals were different, *i.e.*,  $g_{ave} = 2.0075$  (signal I) and  $2.0049$  (signal II), thereby indicating different molecular species. In particular, the greater  $g$  shift in signal I implied a greater contribution of sulfur  $3p_z$  atomic orbitals to the highest occupied molecular orbital (HOMO) at the corresponding molecule; this is because sulfur has a greater spin-orbit coupling than carbon and hydrogen. The calculated molecular  $g$  tensors for DNTT and DBTTF are shown in Table 1. The calculated  $g$  values were consistent with those of signals I and II, as well as with the observation of signal I at a lower gate voltage (Fig. 2): DBTTF ionized more easily than DNTT by attracting hole carriers; this is because the HOMO energy of DBTTF was lower ( $-4.70$  eV) than that of DNTT ( $-5.18$  eV), as depicted in Fig. 1b.

The anisotropy of the  $g$  factors enables the molecular orientations to be determined. DNTT and DBTTF exhibited the highest  $g$  factors along the molecular long axes, as presented in Table 1. The highest  $g$  factors were observed at  $\theta = 90^\circ$  for both signals I and II, as shown in Fig. 3a. This shows that for both DNTT and DBTTF, their molecular long axes should be almost perpendicular to the

substrate. By contrast, two smaller  $g$  factors were observed at  $\theta = 0^\circ$ ; these signals were attributable to those along the two crystal axes within the film plane. Similar features have been observed in uniaxially oriented polycrystalline films of DNNT [20].

For comparison, we conducted angular-dependent FI-ESR measurements of pristine DBTTF FETs [27]. The result indicated a different angular dependence, as shown in Fig. 3d, where the maximum  $g$  factor was recorded at  $\theta = 60^\circ$ – $70^\circ$ . This indicates that the pristine DBTTF formed films with a different crystal structure, in which the molecular long axis of DBTTF was inclined by  $20^\circ$ – $30^\circ$  from the direction normal to the substrate. In fact, DBTTF does not form the layered herringbone packing as is observed in DNNT. The molecular long axis is not perpendicular to the each representative crystallographic plane in any of the polymorphs, according to the crystal structure database [32,33] (BIRKIW in the Cambridge Structural Database). Based on these observations, we conclude that the DBTTF molecules should replace the crystal lattices of DNNT as guest molecules without inducing phase separation.

Figure 3e shows the temperature dependence of the ESR line width of the solid-solution FET at  $\theta = 90^\circ$ , where the variation in  $g$  factors is minimized. The line width of signal II (DNNT site) exhibited significant temperature dependence: the line width decreased (increased) with the increase (decrease) in temperature in the range of 20–120 K (120–285 K). These features were the same as those reported previously for pentacene, DNNT, PB16TTT, and C10-DNBDT-NW FETs and can be explained by motional narrowing (20–120 K) and spin-lattice relaxation mechanisms (120–285 K) [15, 17, 20, 22]. Below 120 K, the line width should be determined by the hyperfine broadening and the motional narrowing effect: the diffusive motion of carriers is thermally activated and averages out the inhomogeneous local magnetic fields due to the hyperfine interactions at each molecular site. This observation provides evidence that the carriers at DNNT sites can propagate via repetitive trap and release processes with average frequencies on the order of  $10^7$ – $10^8$  s<sup>-1</sup> according to the reported procedures [15, 17]. Above 120 K, the line width should be broadened by a short spin-lattice relaxation time, which exceeds the motionally narrowed line width. By contrast, the line width of signal I (DBTTF site) did not indicate a particular temperature dependence over the entire measured temperature range. It is most probable from the results that the line width of signal I should be determined mainly by the hyperfine broadening. In fact, the hyperfine line width is estimated as 60  $\mu$ T, according to the DFT calculations. This is consistent with the carriers at the DBTTF site were less mobile. These observations imply that the current should be transported by the host DNNT crystals, whereas the guest DBTTF molecules should serve as deep trap sites. We note that the ESR spectrum of the pristine DBTTF FETs was more than twice broader than that of signal I in DNNT:DBTTF solid solution over the entire measured temperature range of 5-100 K. We consider that the Elliott-Yafet spin-lattice relaxation should be responsible to determine the FI-ESR linewidth in pristine DBTTF FETs.

The assignment, as presented above, is consistent with the gate voltage dependence or rapid saturation of signal I, as shown in Fig. 2b. The DBTTF sites should be fully occupied by hole carriers at  $V_G = -200$  V. This implies that the saturated carrier density at the DBTTF sites should provide the concentration of guest DBTTF molecules within the DNTT crystals. In fact, the estimated concentration of DBTTF can be regarded as consistent with the ratio of co-evaporation rates among several samples. Hence, we can determine the concentration of DBTTF by integrating the ESR spectra at  $V_G = -200$  V. For example, the DBTTF concentration of the device shown in Fig. 2 was estimated to be 0.2%, based on the density of DNTT molecules per unit area of  $4.2 \times 10^{14} \text{ cm}^{-2}$  [25].

### B. DFT calculations for stable solid-solution formation

The site-selective analyses presented above provide clear evidence that the guest DBTTF molecules randomly replaced the host DNTT molecules in the crystal lattices. To understand the solid-solution formation, we investigated the intermolecular interaction energies of the crystal lattices using DFT calculations. Figure 4a presents a model of the solid-solution crystal, in which the central DNTT molecule is replaced by the guest DBTTF molecules in the herringbone packing of DNTT. We first optimized the herringbone angle and position of the central DBTTF molecule without geometry optimization; subsequently, we optimized the internal geometry of the DBTTF molecule surrounded with DNTT molecules. The sum of the interaction energies of the central DBTTF molecule with the neighboring six DNTT molecules ( $E_{\text{int}}$ ) is shown in Figs. 4b and 4c. Figure 4c shows that the calculated potential contained two minima when the position of the central DBTTF molecule  $R$  was approximately  $\pm 1.4 \text{ \AA}$ . The short S $\cdots$ S contacts between the parallel neighboring molecules resulted in a maximum  $R$  value of approximately  $0.0 \text{ \AA}$ . The  $E_{\text{int}}$  calculated using the optimized geometry was  $-64.8 \text{ kcal/mol}$ . The  $E_{\text{int}}$  calculated using the DNTT and DBTTF crystals were  $-74.5$  and  $-54.9 \text{ kcal/mol}$ , respectively. The  $E_{\text{int}}$  values for the solid-solution model were comparable to these values.

Based on the calculation, we estimated the free energy of mixing  $F_{\text{mix}}$  and the dimensionless interaction parameter  $\chi$  as follows:

$$F_{\text{mix}} = k_B T (x_A \ln x_A + x_B \ln x_B + \chi x_A x_B),$$

$$\chi = \frac{1}{k_B T} (W_{AA} + W_{BB} - 2W_{AB}),$$

where  $k_B$  is the Boltzmann constant;  $T$  is the absolute temperature;  $x_A$  and  $x_B$  are the concentrations of DNTT and DBTTF ( $x_A + x_B = 1$ ), respectively;  $W_{AA}$ ,  $W_{BB}$ , and  $W_{AB}$  are the intermolecular interaction energies per molecule (half of the sum of intermolecular interaction energies of the central molecule with the surrounding six molecules) [7]. The estimation yielded  $F_{\text{mix}} = -0.025 \text{ kcal/mol}$  and  $\chi = -0.17$  for  $x_A = 0.998$  and  $x_B = 0.002$ . Because solid solutions and phase separation were observed when  $\chi \approx 0$  and  $\chi > 2$  [7], this estimation implies that the combination of DNTT and DBTTF is suitable for the formation of a solid solution.

### C. Concentration dependence and correlation to FET characteristics

Figure 5a shows the FI-ESR spectra of six types (A–F) of devices with various concentrations of DBTTF at  $V_G = -200$  V. The concentration of the devices ranged between 0.01%–0.75%, as estimated from FI-ESR spectra. It was observed that most carriers accumulated at the DNNT site in sample A, whereas most accumulated at the DBTTF site in sample F. Figure 5b shows the transfer characteristics for all the devices. We extracted the characteristic parameters from the transfer characteristics, the results of which are shown as a function of DBTTF concentration in Figs. 5c–e. Device A, which had the lowest DBTTF concentration, exhibited the highest mobility of  $0.38 \text{ cm}^2/\text{Vs}$  in the linear regime, the lowest threshold, turn-on voltages at  $V_{\text{th}} = -83$  V and  $V_{\text{on}} = -5$  V, and the smallest subthreshold swing, i.e.,  $SS = 20$  V/decade. It is noteworthy that the relatively high values of  $V_{\text{th}}$ ,  $V_{\text{on}}$ , and  $SS$  were ascribed to the low specific capacitance of the gate insulator of parylene, i.e.,  $4.5 \text{ nF cm}^{-2}$ , which was adopted to perform sensitive and reproducible FI-ESR measurements.

As the DBTTF concentration increased, the nominal field-effect mobility decreased (Fig. 5c). However, the decrease occurred partly because the mobility was estimated in the subthreshold regime for devices C–F. According to the literature, guest molecules can be categorized into two types: those that induce and do not induce the distortion of surrounding molecules. The former results in many physical traps in the crystals, which yields a significant reduction in the carrier mobility, whereas the latter forms a solid solution and barely affects the mobility. The result of the current study can be categorized into the latter case; this is supported by the parallel molecular orientations of DNNT and DBTTF, as observed in the angle-dependent FI-ESR spectra shown in Fig. 3.

The increase in the DBTTF concentration increased the threshold voltage, turn-on voltage, and  $SS$ . These effects can be scrutinized using the deep trap model [2]. In general, deep traps cause a shift in the threshold voltage by  $\Delta V = eN_{\text{trap}}/C$ , where  $e$  is the elementary charge,  $N_{\text{trap}}$  the trap density per unit area, and  $C$  the capacitance of the gate insulator per unit area. When we assume that  $N_{\text{trap}}$  is the same as the density of DBTTF molecules per unit area, voltage shifts are expected, as indicated by the red lines in Fig. 5d. The expected voltage shift is quantitatively consistent with the observations. However, we discovered that the threshold voltage indicated a significant offset at a DBTTF concentration of 0%. We speculate that this large threshold voltage originated from the DNNT films, such as lattice defects or grain boundaries, or from the semiconductor/insulator interface, such as dipole fluctuations on the surface of the gate insulator. The  $SS$  indicated an approximately linear dependence on the DBTTF concentration, which is consistent with theory [34]. Hence, the DNNT:DBTTF solid solution can be regarded as a model system that can be used to investigate the intrinsic effect of carrier trapping by guest molecules with discrimination from other structural effects. Although the effect on the device performance should be governed by the combination of molecular species, it is natural to assume that impurities with a higher ionisation energy (or a lower electron

affinity for *n*-type) than that of the host material should impose less effects because they do not trap but only scatter carriers, whereas those that induce structural distortions should impose more significant effects on the mobility.

#### IV. CONCLUSION

We demonstrated a method for investigating the effect of guest molecules in solid-solution organic FETs under operation. The method provides a microscopic view of molecular species, molecular orientations, carrier densities, and carrier dynamics. The measurements of device properties at different guest concentrations revealed desirable field-effect mobilities; however, the threshold and turn-on voltages exhibited considerable shifts, which can be explained using a simple deep trap model. The obtained molecular orientations and the desirable field-effect mobilities implied the feasibility of the DNTT:DBTTF solid solution as a model system for investigating the effects of impurities on organic FETs.

Finally, the operando FI-ESR technique offers several unique advantages for investigating the effects of impurities in organic FETs. First, it allows the molecular orientations of minority molecules to be determined. Second, its highly sensitive nature allows a small amount of guest molecules to be detected; in this regard, its minimum sensitivity is 0%. Third, it can selectively detect carrier dynamics at respective molecular sites and discriminate whether the respective sites are traps. It is noteworthy that the FI-ESR technique can be used to directly determine the transport characteristics, unlike conventional impurity analyses of source semiconducting materials.

#### Acknowledgements

The polyethylene naphthalate substrates (Q65F, TEONEX) were supplied by Dupont. This work was partly supported by JSPS KAKENHI (Grant No. 18H01855) and by JST CREST (Grant No. JPMJCR18J2). We would like to thank Editage ([www.editage.com](http://www.editage.com)) for English language editing.

#### References

- [1] H. Sirringhaus, Device physics of solution-processed organic field-effect transistors, *Adv. Mater.* **17**, 2411-2425 (2005).
- [2] M. E. Gershenson, V. Podzorov and A. F. Morpurgo, Colloquium: Electronic transport in single-crystal organic transistors, *Rev. Mod. Phys.* **78**, 973 (2006).
- [3] C. Reese and Z. Bao, Organic single-crystal field-effect transistors, *Materials Today* **10**, 20-27 (2007).
- [4] H. Klauk, Organic thin-film transistors, *Chem. Soc. Rev.* **39**, 2643-2666 (2010).
- [5] A. F. Paterson, S. Singh, K. J. Fallon, T. Hodsdon, Y. Han, B. C. Schroeder, H. Bronstein, M. Heeney, I. McCulloch and T. D. Anthopoulos, Recent progress in high-mobility organic transistors: A reality check, *Adv. Mater.* **30**, 1801079 (2018).
- [6] B. Lussem, C.-M. Keum, D. Kasemann, B. Naab, Z. Bao and K. Leo, Doped organic transistors, *Chem. Rev.* **116**, 13714-13751 (2016).
- [7] A. Hinderhofer and F. Schreiber, Organic-organic heterostructures: Concepts and applications, *ChemPhysChem* **13**, 628-643 (2012).
- [8] A. Opitz, J. Wagner, W. Brütting, A. Hinderhofer and F. Schreiber, Molecular semiconductor blends:

- Microstructure, charge carrier transport, and application in photovoltaic cells, *physica status solidi (a)* **206**, 2683-2694 (2009).
- [9] J. Dieterle, K. Broch, A. Hinderhofer, H. Frank, J. Novak, A. Gerlach, T. Breuer, R. Banerjee, G. Witte and F. Schreiber, Structural properties of picene–perfluoropentacene and picene–pentacene blends: Superlattice formation versus limited intermixing, *J. Phys. Chem. C* **119**, 26339-26347 (2015).
- [10] K. Broch, A. Aufderheide, L. Raimondo, A. Sassella, A. Gerlach and F. Schreiber, Optical properties of blends: Influence of mixing-induced disorder in pentacene: Diindenoperylene versus perfluoropentacene: Diindenoperylene, *J. Phys. Chem. C* **117**, 13952-13960 (2013).
- [11] D. Lubert-Perquel, E. Salvadori, M. Dyson, P. N. Stavrinou, R. Montis, H. Nagashima, Y. Kobori, S. Heutz and C. W. M. Kay, Identifying triplet pathways in dilute pentacene films, *Nature Comm.* **9**, 4222 (2018).
- [12] X. Xu, T. Xiao, X. Gu, X. Yang, S. V. Kershaw, N. Zhao, J. Xu and Q. Miao, Solution-processed ambipolar organic thin-film transistors by blending p-and n-type semiconductors: Solid solution versus microphase separation, *ACS Appl. Mater. Interf.* **7**, 28019-28026 (2015).
- [13] S. Arai, S. Inoue, T. Hamai, R. Kumai and T. Hasegawa, Semiconductive single molecular bilayers realized using geometrical frustration, *Adv. Mater.* **30**, 1707256 (2018).
- [14] K. Marumoto, S. Kuroda, T. Takenobu and Y. Iwasa, Spatial extent of wave functions of gate-induced hole carriers in pentacene field-effect devices as investigated by electron spin resonance, *Phys. Rev. Lett.* **97**, 256603 (2006).
- [15] H. Matsui, T. Hasegawa, Y. Tokura, M. Hiraoka and T. Yamada, Polaron motional narrowing of electron spin resonance in organic field-effect transistors, *Phys. Rev. Lett.* **100**, 126601 (2008).
- [16] H. Tanaka, S. Watanabe, H. Ito, K. Marumoto and S. Kuroda, Direct observation of the charge carrier concentration in organic field-effect transistors by electron spin resonance, *Appl. Phys. Lett.* **94**, 82 (2009).
- [17] H. Matsui, A. S. Mishchenko and T. Hasegawa, Distribution of localized states from fine analysis of electron spin resonance spectra in organic transistors, *Phys. Rev. Lett.* **104**, 056602 (2010).
- [18] K. Marumoto, N. Arai, H. Goto, M. Kijima, K. Murakami, Y. Tominari, J. Takeya, Y. Shimoi, H. Tanaka, S. Kuroda *et al.*, Microscopic mechanisms behind the high mobility in rubrene single-crystal transistors as revealed by field-induced electron spin resonance, *Phys. Rev. B* **83**, 075302 (2011).
- [19] A. S. Mishchenko, H. Matsui and T. Hasegawa, Distribution of localized states from fine analysis of electron spin resonance spectra of organic semiconductors: Physical meaning and methodology, *Phys. Rev. B* **85**, 085211 (2012).
- [20] H. Matsui, D. Kumaki, E. Takahashi, K. Takimiya, S. Tokito and T. Hasegawa, Correlation between interdomain carrier hopping and apparent mobility in polycrystalline organic transistors as investigated by electron spin resonance, *Phys. Rev. B* **85**, 035308 (2012).
- [21] H. Tanaka, M. Hirate, S. Watanabe, K. Kaneko, K. Marumoto, T. Takenobu, Y. Iwasa and S. Kuroda, Electron spin resonance observation of charge carrier concentration in organic field-effect transistors during device operation, *Phys. Rev. B* **87**, 045309 (2013).
- [22] J. Tsurumi, H. Matsui, T. Kubo, R. Hausermann, C. Mitsui, T. Okamoto, S. Watanabe and J. Takeya, Coexistence of ultra-long spin relaxation time and coherent charge transport in organic single-crystal semiconductors, *Nature Phys.* **13**, 994-998 (2017).
- [23] S. Iguchi, Y. Sakurai, N. Fujita, F. Osawa and K. Marumoto, Electrically controllable spin states of holes and electrons in organic semiconductor materials, *ACS Appl. Electron. Mater.* **1**, 2522-2530 (2019).
- [24] W. Baker, T. Keevers, J. Lupton, D. McCamey and C. Boehme, Slow hopping and spin dephasing of coulombically bound polaron pairs in an organic semiconductor at room temperature, *Phys. Rev. Lett.* **108**, 267601 (2012).
- [25] T. Yamamoto and K. Takimiya, Facile synthesis of highly  $\pi$ -extended heteroarenes, dinaphtho[2,3-b:2',3'-f]chalcogenopheno[3,2-b]chalcogenophenes, and their application to field-effect transistors, *J. Am. Chem. Soc.* **129**, 2224-2225 (2007).
- [26] S. Haas, Y. Takahashi, K. Takimiya and T. Hasegawa, High-performance dinaphtho-thieno-thiophene single crystal field-effect transistors, *Appl. Phys. Lett.* **95**, 022111 (2009).
- [27] T. Yamada, T. Hasegawa, M. Hiraoka, H. Matsui, Y. Tokura and G. Saito, Control of film morphology and its effects on subthreshold characteristics in dibenzotetrathiafulvalene organic thin-film transistors, *Appl. Phys. Lett.* **92**, 210 (2008).
- [28] M. J. Frisch, G. W. Trucks, H. B. Schlegel, G. E. Scuseria, M. A. Robb, J. R. Cheeseman, G. Scalmani, V. Barone, G. A. Petersson, H. Nakatsuji *et al.*, Gaussian 16, Revision C.01 (Wallingford, CT, 2016).

- [29] S. Grimme, J. Antony, S. Ehrlich and H. Krieg, A consistent and accurate ab initio parametrization of density functional dispersion correction (DFT-D) for the 94 elements H-Pu, *J. Chem. Phys.* **132**, 154104 (2010).
- [30] B. J. Ransil, Studies in molecular structure. Iv. Potential curve for the interaction of two helium atoms in single-configuration lcao mo scf approximation, *J. Chem. Phys.* **34**, 2109-2118 (1961).
- [31] S. Boys and F. Bernardi, Molecular physics: An international journal at the interface between chemistry and physics, *Mol. Phys* **19**, 553-566 (1970).
- [32] C. R. Groom, I. J. Bruno, M. P. Lightfoot and S. C. Ward, The cambridge structural database, *Acta Crystallographica Section B: Structural Science, Cryst. Eng. Mater.* **72**, 171-179 (2016).
- [33] The Cambridge Structural Database, identifier: BIRKIW, <https://www.ccdc.cam.ac.uk/structures/Search?Ccdcid=BIRKIW&DatabaseToSearch=Published>
- [34] W. L. Kalb and B. Batlogg, Calculating the trap density of states in organic field-effect transistors from experiment: A comparison of different methods, *Phys. Rev. B* **81**, 035327 (2010).

Table 1. DFT calculation of molecular g tensor. Directions of principle axes are shown in Fig. 1c. Experimental g factors for mixed film are shown.

molecule	calculation				experimental				
	$g_x$	$g_y$	$g_z$	average	signal	$\theta = 90^\circ$	$\theta = 0^\circ$		average
DBTTF	2.0069	2.0156	2.0019	2.0081	I	2.0148 $\pm 0.0001$	2.0059 $\pm 0.0002$	2.0032 $\pm 0.0002$	2.0080 $\pm 0.0001$
DNTT	2.0034	2.0061	2.0025	2.0040	II	2.0092 $\pm 0.0002$	2.0036 $\pm 0.0003$	2.0019 $\pm 0.0003$	2.0049 $\pm 0.0002$

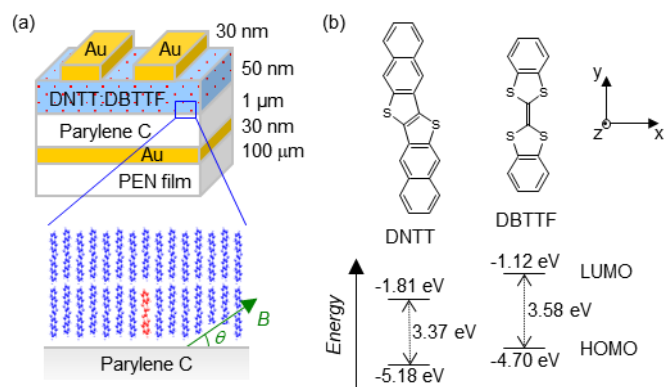


Figure 1. a) Device structure of DNTT:DBTTF field-effect transistors (FETs). Static magnetic field was applied at angle  $\theta$  with respect to substrate plane. b) Molecular structures and HOMO–LUMO levels of DNTT and DBTTF molecules. Coordinates indicate principal axes of g tensor. Energies were calculated using Gaussian 16, based on density functional theory (DFT) with B3LYP functional and 6-31G(d) basis set.

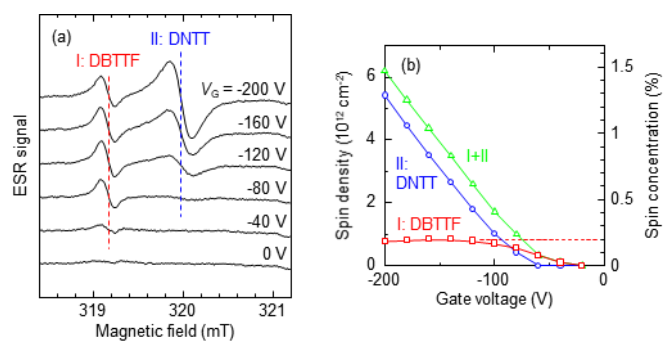


Figure 2. a) Field-induced ESR spectra of DNTT (99.8%):DBTTF (0.2%) FET. b) Density of spins accumulated at DNTT and DBTTF molecules, separately. Right axis indicates corresponding spin concentration relative to number of DNTT molecules in first layer.

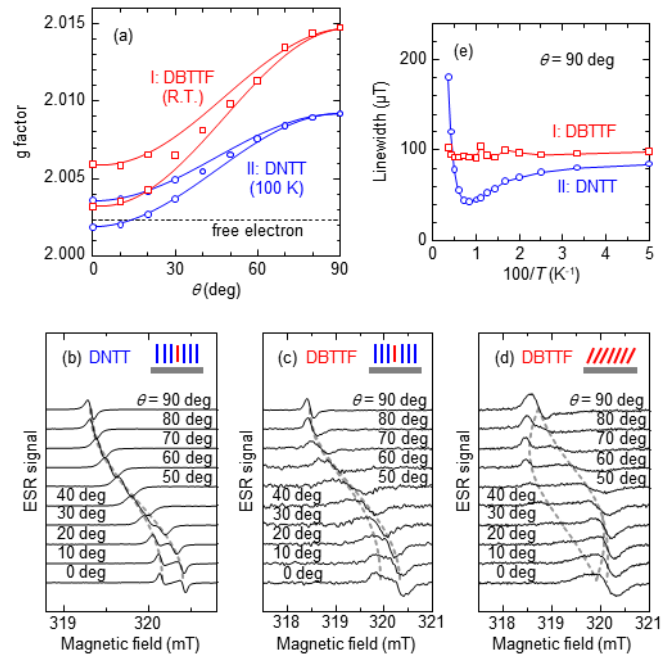


Figure 3. a) Angle dependence of  $g$  factor for DNTT and DBTTF components in DNTT:DBTTF FET. b) Angle-dependent ESR spectra of DNTT component in DNTT:DBTTF FET at  $V_G = -200$  V at 100 K. c) Angle-dependent ESR spectra of DBTTF component in DNTT:DBTTF FET at  $V_G = -60$  V at room temperature. d) Angle-dependent ESR spectra of pristine DBTTF FET at  $V_G = -200$  V at 5 K. Insets show schematic illustrations of molecular orientation on substrates of DNTT:DBTTF and pristine DBTTF FETs. Dashed lines in b), c), and d) provide visual guide. e) Temperature dependence of line width for DNTT and DBTTF components in DNTT:DBTTF FET.

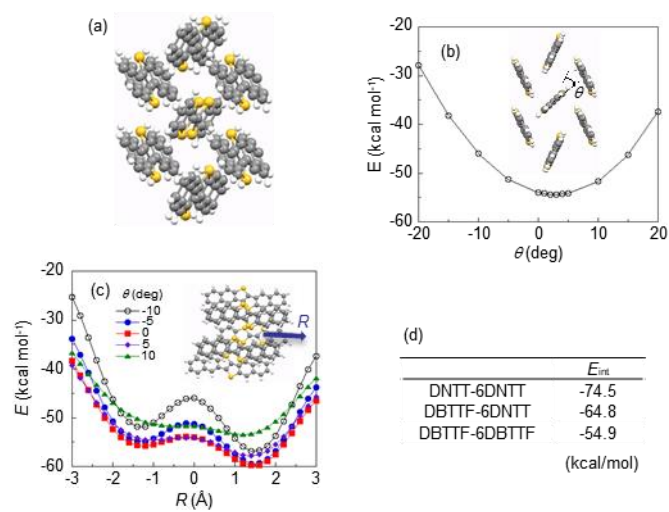


Figure 4. a) Optimized model of solid-solution crystal, which was obtained by replacing central DNTT molecule with guest DBTTF molecule in herringbone packing of DNTT. b) Changes in sum of intermolecular interaction energies of DBTTF molecule with six surrounding DNTT molecules ( $E_{int}$ ) associated with change in herringbone angle. c) Changes in  $E_{int}$  associated with change in position of central DBTTF molecule. d)  $E_{int}$  calculated using crystal structures of DNTT and DBTTF and that calculated using optimized geometry of solid-solution crystal model.

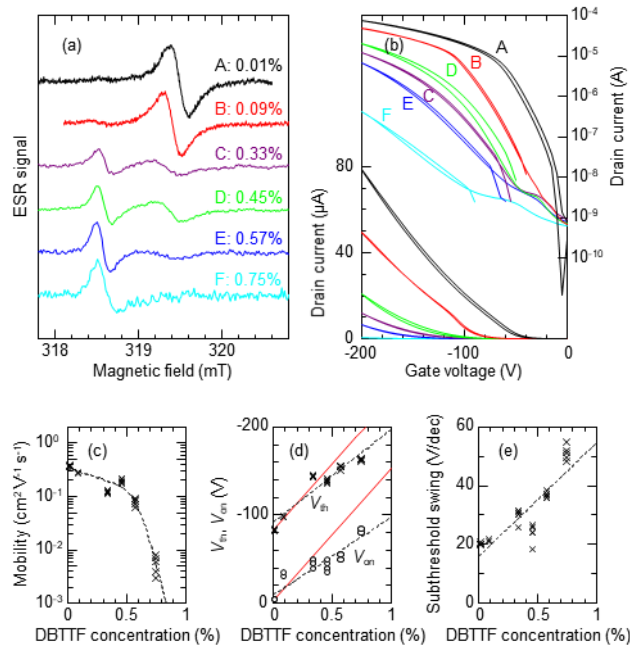


Figure 5. a) Field-induced ESR spectra of DNTT:DBTTF FETs with different DBTTF concentrations. Gate voltage was fixed at  $-200$  V, and temperature was room temperature. Concentration of DBTTF was determined via ESR measurement. b) Transfer characteristics of devices at room temperature. Channel length  $L = 0.5$  mm, channel width  $W = 20$  mm, and drain voltage  $V_D = -10$  V. c) Field-effect mobility, d) threshold and turn-on voltages, and e) subthreshold swing of devices. Dashed lines provide visual guide. Solid lines show calculated slope obtained based on simple assumption of charge accumulation in first monolayer.